PAG1 directs SRC-family kinase intracellular localization to mediate receptor tyrosine kinase-induced differentiation

Lauren Foltz[a], Juan Palacios-Moreno[b], Makenzie Mayfield[a], Shelby Kinch[a], Jordan Dillon[a], Jed Syrenne[a], Tyler Levy[c], and Mark Grimes[a,*]

[a]Division of Biological Sciences, Center for Biomolecular Structure and Dynamics, and Center for Structural and Functional Neuroscience, University of Montana, Missoula, MT 59812; [b]University of Minnesota Medical School, Duluth, MN 55812; [c]Cell Signaling Technology, Danvers, MA 01923

ABSTRACT **All receptor tyrosine kinases (RTKs) activate similar downstream signaling pathways through a common set of effectors, yet it is not fully understood how different receptors elicit distinct cellular responses to cause cell proliferation, differentiation, or other cell fates. We tested the hypothesis that regulation of SRC family kinase (SFK) signaling by the scaffold protein, PAG1, influences cell fate decisions following RTK activation. We generated a neuroblastoma cell line expressing a PAG1 fragment that lacks the membrane-spanning domain (PAG1^{TM-}) and localized to the cytoplasm. PAG1^{TM-} cells exhibited higher amounts of active SFKs and increased growth rate. PAG1^{TM-} cells were unresponsive to TRKA and RET signaling, two RTKs that induce neuronal differentiation, but retained responses to EGFR and KIT. Under differentiation conditions, PAG1^{TM-} cells continued to proliferate and did not extend neurites or increase β-III tubulin expression. FYN and LYN were sequestered in multivesicular bodies (MVBs), and dramatically more FYN and LYN were in the lumen of MVBs in PAG1^{TM-} cells. In particular, activated FYN was sequestered in PAG1^{TM-} cells, suggesting that disruption of FYN localization led to the observed defects in differentiation. The results demonstrate that PAG1 directs SFK intracellular localization to control activity and to mediate signaling by RTKs that induce neuronal differentiation.**

Monitoring Editor
Carl-Henrik Heldin
Ludwig Institute for Cancer Research

Received: Feb 24, 2020
Revised: Jul 15, 2020
Accepted: Jul 21, 2020

INTRODUCTION

Precise temporal and spatial control over cell signaling pathways is necessary to coordinate diverse cell responses to extracellular signals (Irannejad *et al.*, 2015; Bergeron *et al.*, 2016; Lemmon *et al.*, 2016). Receptor tyrosine kinases (RTKs) initiate intracellular signaling pathways after binding extracellular ligands at the plasma membrane, which typically induces receptor homodimerization and transphosphorylation of tyrosine residues on the cytoplasmic tail of dimer partners (Lemmon and Schlessinger, 2010). Phosphorylated tyrosine residues on RTKs act as platforms for the recruitment of adaptor proteins to activate four downstream canonical cell signaling pathways: RAS/MAPK, PI3K, PLC-γ, and SRC Family Kinases (SFKs). Different RTKs elicit different cell responses, however, and not all RTKs activate each pathway to the same extent (Marshall, 1995; Chen *et al.*, 2012b). How different receptors initiate and terminate a cascade of effector signals with precise sequence and timing to elicit a particular cell response remains unclear.

The SFK familly comprises nine members in humans: SRC, YES1, FYN, FGR, FRK, LYN, BLK, HCK, and LCK. SFKs have a modular domain structure and are composed of a unique N-terminal region termed the SRC Homology 4 domain (SH4), an SH3 domain, an SH2 domain, an SH1 catalytic/kinase domain, and a short regulatory tail. SH2 and SH3 domains bind to phosphorylated tyrosine residues

This article was published online ahead of print in MBoC in Press (http://www.molbiolcell.org/cgi/doi/10.1091/mbc.E20-02-0135) on July 29, 2020.
*Address correspondence to: Mark Grimes (Mark.Grimes@mso.umt.edu).
Abbreviations used: AGC, automatic gain control; bRP, basic reverse phase; BSA, bovine serum albumin; CSK, C-terminal SRC kinase; CST, Cell Signaling Technology; DRM, detergent-resistant membrane; DTT, dithiothreitol; FBS, fetal bovine serum; FDR, false discovery rate; GRI, growth rate index; IP, immunoprecipitation; LC-MS, liquid chromatography mass spectrometry; Lys, lysosome; MVB, multivesicular body; NCE, normalized collision energy; NGF, nerve growth factor; PAG1, phosphoprotein associated with glycosphingolipid enriched-microdomains 1; PBS, phosphate-buffered saline; RA, retinoic acid; RTK, receptor tyrosine kinase; SFK, SRC Family Kinase; SH, SRC homology; TCA, trichloroacetic acid; TfR, transferrin receptor; TMT, tandem-mass-tag; WT, wild type.

and proline-rich regions, respectively (Mayer, 2015). This domain structure, similar to SH2/SH3 adaptor proteins, links SFKs to a large interactome tuned to phosphotyrosine signals, propagated through their tyrosine kinase activity, which is governed by both activating and inhibitory phosphorylation (Harrison, 2003; Pawson, 2004; Sandilands and Frame, 2008). Myristoylation and palmitoylation on the N-terminal region recruits SFKs to membrane surfaces, including the plasma membrane, endosomes, Golgi, and endoplasmic reticulum, although a pool of SFKs remains cytosolic (Alland *et al.*, 1994; Hantschel *et al.*, 2003). SFKs are thus signaling hubs whose activity can be placed on a variety of intracellular membranes to link upstream RTK signaling to the appropriate effector pathways.

Our previous work pointed to the dynamic intracellular localization of two members of the SRC family of tyrosine kinases, FYN and LYN, as potential means to control RTK effector pathways in cells from the neural crest-derived cancer, neuroblastoma. In a phosphoproteomic study, we combined fractionation of membrane compartments including endosomes and detergent-resistant lipid rafts (McCaffrey *et al.*, 2009; Pryor *et al.*, 2012) with large scale analysis of 21 neuroblastoma cell lines (Palacios-Moreno *et al.*, 2015). Neuroblastoma cells express more than half of the RTKs in the human genome, which suggests that mechanisms to discern different receptors' signals, and integrate them when more than one receptor is activated, must play a role in cell fate decisions in neural crest and neuroblastoma, as for other tissues in multicellular organisms (Iglesias-Bartolome and Gutkind, 2011; Chen *et al.*, 2012a; Schwarz *et al.*, 2012; Theveneau and Mayor, 2012). Different RTKs were enriched in endosomes and lipid rafts in different cell lines (Palacios-Moreno *et al.*, 2015). Similarly, SFK family members, mainly FYN and LYN (and to a lesser extent SRC and YES1), phosphorylated on both activating and inhibitory sites, were enriched in different endosome populations and plasma membrane fractions with distinct distributions in different neuroblastoma cell lines (Palacios-Moreno *et al.*, 2015). FYN and LYN activity and localization change in response to activation from different RTKs, which suggests that a mechanism must exist to tailor SFK relocalization to elicit a particular response (Palacios-Moreno *et al.*, 2015).

We also observed enrichment of PAG1 (phosphoprotein associated with glycosphingolipid-enriched microdomains 1) in both endosomes and lipid rafts (Palacios-Moreno *et al.*, 2015). PAG1 is a scaffold protein composed of a very short extracellular N-terminal domain, a transmembrane domain, and a long intracellular cytoplasmic domain. PAG1's cytoplasmic tail is rich in phosphorylation sites and potential docking sites for interactions with SFKs, phosphatases, and trafficking machinery (Barua *et al.*, 2012). PAG1 binds SFKs and regulates their activity by facilitating the interaction with C-terminal SRC kinase (CSK) (Kawabuchi *et al.*, 2000; Ingley *et al.*, 2006; Oneyama *et al.*, 2008; Lindquist *et al.*, 2011). Docking of both CSK and SFKs on PAG1 brings them in proximity where CSK phosphorylates SFKs on C-terminal inhibitory tyrosine residues (Lindquist *et al.*, 2003; Solheim *et al.*, 2008a; Saitou *et al.*, 2014). Due to its known functions and presence in lipid rafts and endosomes, we hypothesized that PAG1 may direct SFK intracellular location as well as activity, and that this mechanism may play a role in distinguishing cell signaling responses to different receptors.

Here we investigate cell signaling mechanisms that distinguish RTK signals that cause proliferation versus differentiation in neuroblastoma cell lines. We show that generation of a neuroblastoma cell line expressing a PAG1 mutant lacking the transmembrane domain (PAG1^{TM-}) resulted in enhanced tumorigenic phenotypes: anchorage-independent growth and proliferation. PAG1^{TM-}-expressing cells failed to respond to differentiative signaling, while maintaining responses to oncogenic receptors. We show that cells sequestered FYN and LYN in the lumen of multivesicular bodies (MVBs), and that this process was disrupted in PAG1^{TM-} cells, which exhibited high amounts of active FYN, and inactive LYN, sequestered in MVBs. Our findings indicate that PAG1 regulates the intracellular localization and activity of FYN and LYN to convey signaling instructions from RTKs that cause neuronal differentiation.

RESULTS

To examine the role of PAG1 in SFK regulation, we aimed to generate human neuroblastoma PAG1 knockout cell lines using lentiviral delivery of CRISPR/Cas9 plasmids. Sequencing results after transduction and selection of SH-SY5Y cells indicated a heterozygous frame shift mutation in Exon 5 of the PAG1 gene that resulted in a stop codon shortly downstream (Figure 1, A and B). We expected reduced expression; however, a mutant PAG1 protein that lacks the transmembrane domain was detected by Western blot and mass spectrometry analysis (PAG1^{TM-}; Figure 1C). This protein was not bound to membranes, was absent in endosomes, and strictly located to cytosol fractions (Figure 1D). WT PAG1 was localized in endosome fractions that migrated to the lower half of the gradient (Figure 1D). The data suggest that the soluble, cytoplasmic PAG1^{TM-} protein was translated starting from one of two downstream methionine residues that have Kozak consensus sequences and predicted protein products that are truncations of the wild-type (WT) protein (Wang *et al.*, 2002; Mou *et al.*, 2017; Sharpe and Cooper, 2017). All PAG1 peptides identified by mass spectrometry lie within the range of the predicted truncated protein (Supplemental Table S1).

We hypothesized that PAG1^{TM}-expressing cells would have disrupted regulation of SFKs and other signaling proteins downstream of RTK signaling. To test this, we determined the SFK activation status of individual neuroblastoma cells using flow cytometry. We assessed total SFK phosphorylation using an antibody that recognizes the activating phosphorylation site (pY416), and found that the PAG1^{TM-} cell population had nearly twice the amount of active SFKs compared with WT cells (Figure 1E), suggesting that the mutant PAG1 is deficient in its ability to control SFK activity. The generation of PAG1^{TM-}-expressing cells presented a unique opportunity to study the effect of dysregulated SFK activity on cell growth, differentiation, and cell signaling pathways, without directly affecting SFK structure or binding capabilities.

PAG1^{TM-} enhanced growth rate in neuroblastoma cells and reduced the effect of the SFK inhibitor PP2

To compare the growth of PAG1^{TM-} and WT SH-SY5Y cells, we employed the MTT assay, which determines cell growth by measuring mitochondrial enzyme activity. PAG1^{TM-} grew faster than WT SH-SY5Y cells (Figure 2A). Because growth rate measurements have been shown to fluctuate, even within the same cell line, we used a more robust method described by Hafner *et al.* (2016) to compare growth rates. In the equation described by Hafner *et al.* (2016), growth rate index (GRI) = $2^{(R'/R)}$–1, where R = WT growth rate and R' = PAG1^{TM-} growth rate (see complete formulae in *Materials and Methods*). A GRI of median 2.9, mean 4.5 clearly indicates that PAG1^{TM-} cells grow faster than WT cells (Figure 2B). To further characterize changes in proliferation rate due to overactive SFK signaling, we treated cells with a small molecule SFK inhibitor, PP2. PP2 is very active against LCK and FYN, but less active against SRC and

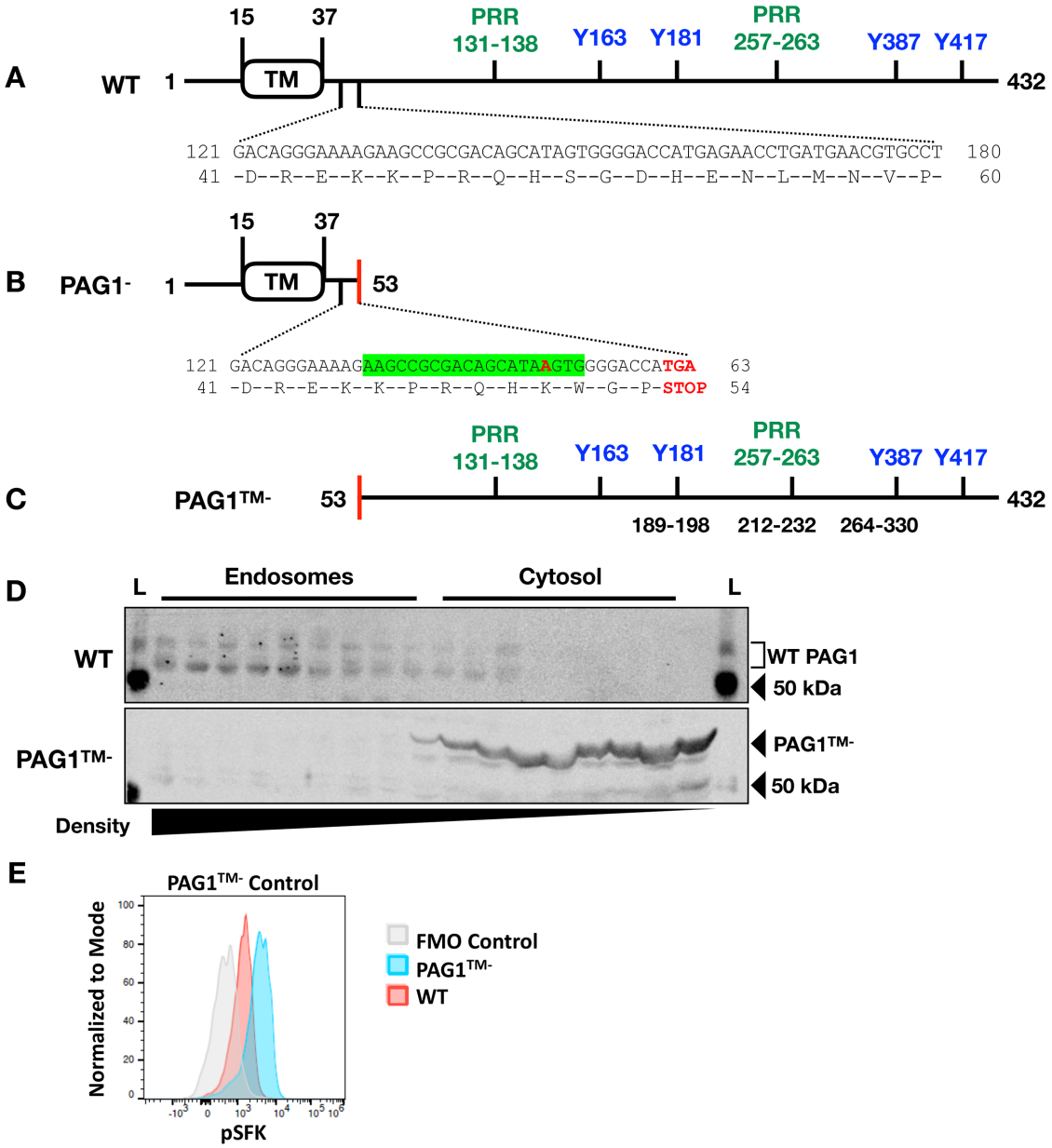

FIGURE 1: SH-SY5Y cells expressing cytosolic PAG1 (PAG1^{TM-}) were generated using CRISPR/Cas9. (A) WT PAG1 has a small extracellular N-terminal region, transmembrane domain (TM), and long intracellular C-terminal tail. Several phosphorylated residues and proline-rich regions (PRR, PXXP motif, green) act as docking sites for protein–protein interactions. Phosphorylated Y163/Y181 and Y387/417 (blue) are binding sites for FYN and LYN SH2 domains, respectively (Ingley *et al.*, 2006; Solheim *et al.*, 2008a, b; Barua *et al.*, 2012). (B) CRISPR sgRNA recognition site is highlighted in green. Sequencing results indicated a single base pair insertion that resulted in a stop codon to generate a heterozygous PAG1^{-} SH-SY5Y cell line (red). (C) Met residues upstream of the detected peptides act as alternate translation start sites to produce the cytosolic PAG1 product (PAG1^{TM-}). PAG1 peptides were detected via mass spectrometry on PAG1^{-} cell lines (amino acid numbers are indicated in black). (D) Organelle fractionation comparing the endosomal distribution of WT PAG1 vs. PAG1^{TM-}. Fractions were taken from 25% to 2.5% iodixanol gradients and decrease in density from left to right. L, biotinylated ladder. PAG1 is extensively posttranslationally modified in WT cells and displays multiple bands on Western blots; in PAG1^{TM-}, a single band is visible, suggesting few such modifications. (E) Levels of activated SFKs were increased in PAG1^{TM-}-expressing SH-SY5Ys (blue) compared with WT SH-SY5Y cells (red). Cells were stained with a pSFK antibody recognizing the activating phosphorylation site conserved in several SFKs, and pSFK fluorescence was measured by flow cytometry. Results are representative of at least three independent experiments.

LYN (Hanke *et al.*, 1996; Brandvold *et al.*, 2012). Figure 2C compares the growth rates of WT and PAG1^{TM-} cells treated with PP2 compared with their respective vehicle controls. The data indicate that PP2 did not greatly affect the growth rate of PAG1^{TM-} cells, but did significantly reduce WT cell growth (Figure 2C, WT GRI < 0.6 at 5 and 0.5 μM PP2). Since PAG1^{TM-} cells had increased SFK activity and were less sensitive to the SFK inhibitor PP2 than WT cells, this suggests that disruption of PAG1 function probably affects more than one SFK, and that PP2-sensitive SFKs are not driving cell proliferation in PAG1^{TM-} cells.

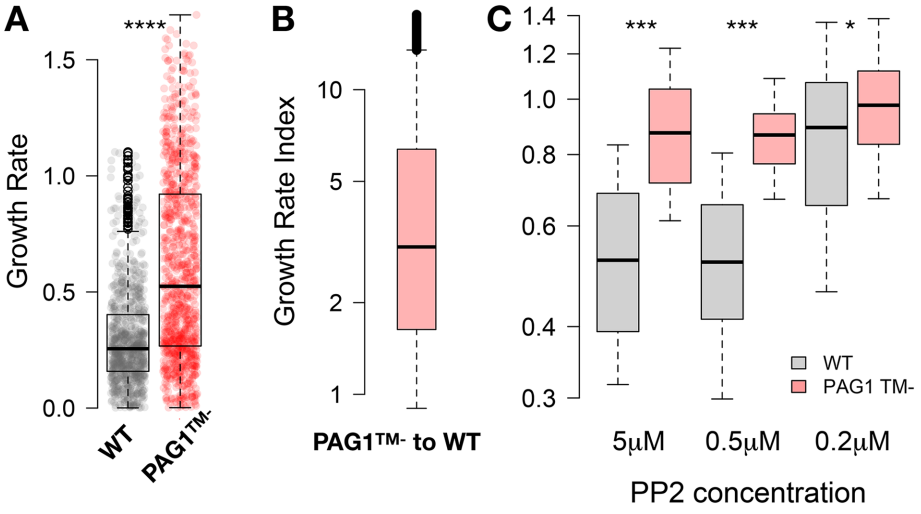

FIGURE 2: PAG1™- expression enhanced growth rate and desensitized cells to the SFK inhibitor PP2. (A) Box plots of MTT growth rates with individual data points shown from WT SY5Y and PAG1^{TM-} cells. (B, C) GRI was calculated as described in Hafner *et al.* (2016; described in *Materials and Methods*). (B) GRIs comparing SY5Y WT to PAG1^{TM-} cells. (C) GRIs calculated from SY5Y WT (gray) and PAG1^{TM-} (red) cells treated with PP2 at the indicated concentrations. The *p* values from 8 (A, B) or 5 (C) independent experiments are indicated: *< 0.05, *** <0.0005, ****< 2.2×10^{-16} (Welch two-sample *t* test).

PAG1^{TM-} cells exhibited increased anchorage-independent growth

We next asked whether PAG1^{TM-} expression contributed to the gain of transformed tumorigenic phenotypes as measured by colony growth in soft agar. PAG1^{TM-} cells exhibited increased colony formation in soft agar compared with WT cells (Figure 3, A and B). Cells expressing PAG1^{TM-} formed more total colonies than WT cells, and PAG1^{TM-} colonies were much larger, consistent with the increased cell division noted above. PP2 treatment did not significantly affect colony formation for PAG1^{TM-}-expressing cells, but did decrease the number and size of colonies formed by WT cells (Figure 3A). These findings are consistent with previously reported experiments using siRNA knockdown of PAG1 (Oneyama *et al.*, 2008; Agarwal *et al.*, 2016).

PAG1^{TM-} prevented differentiation of SH-SY5Y neuroblastoma cells

Different RTKs induce distinct cell fate decisions that are mediated by SFK signaling and other pathways. Because increases in tumorigenicity and proliferation are typically accompanied by deficits in differentiation, we hypothesized that disrupting SFK activation by expression of the PAG1^{TM-} mutant would also disrupt differentiation. We used neurite extension and expression of β-III tubulin as assays for differentiation. We measured neurite length after exposing cells to a combination of retinoic acid (RA) and nerve growth factor (NGF), which induces neuronal differentiation in neuroblastoma cell lines (Shipley *et al.*, 2016). SH-SY5Y cells normally respond to these ligands by slowing cell division and extending neurites (Figure 4, A and B). PAG1^{TM-}-expressing cells did not extend neurites under differentiation conditions, whereas control SH-SY5Ys displayed significant increases in neurite length (Figure 4A). Similarly, we assessed cellular levels of β-III tubulin by flow cytometry after growth in differentiation-inducing media. β-III tubulin is a neuron-specific tubulin whose expression is induced by neuronal differentiation (Figure 4C; Guo *et al.*, 2010). PAG1^{TM-} cells did not increase β-III tubulin expression after exposure to differentiation conditions (blue), whereas WT cells displayed robust induction of expression (red; Figure 4C). The normal slowing of the cell division cycle on differentiation was also disrupted in mutant cells. While the majority of WT cells remained in G0/G1, PAG1^{TM-} cells had higher percentages of cells in S and G2/M stages of the cell cycle while exposed to these differentiation conditions, suggesting frequent cell division (Figure 4, D and E). These results suggest that PAG1^{TM-} SH-SY5Ys are not capable of inducing cell signaling mechanisms that promote neuronal differentiation.

PAG1^{TM-} expression increased ERK activation in response to EGF

Because PAG1^{TM-} cells exhibited enhanced growth rate and defects in differentiation, we hypothesized that downstream cell signaling responses to different RTKs would reflect these characteristics. We asked whether changes in SFK signaling by PAG1^{TM-} expression affected the activation of the RAS/MAPK pathway. We assessed the activation of ERK and SFKs for both WT and PAG1^{TM-}-expressing SH-SY5Y

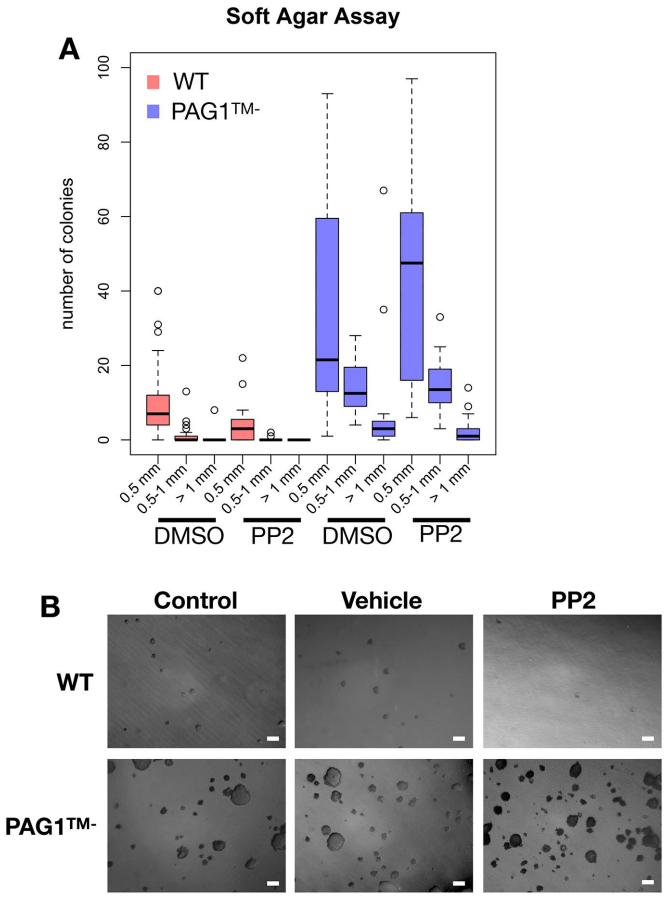

FIGURE 3: PAG1^{TM-} enhanced anchorage-independent growth. (A) Soft agar assay of WT vs. PAG1^{TM-}-expressing SH-SY5Y cells. After 7 d, control or PP2-treated (5 μM) cells were imaged and colony sizes were binned into three categories (0.5 mm^2, 0.5–1 mm^2, and 1 mm^2), $n = 3$. (B) Representative images of colonies quantified in A for each condition. Scale bar = 1 mm.

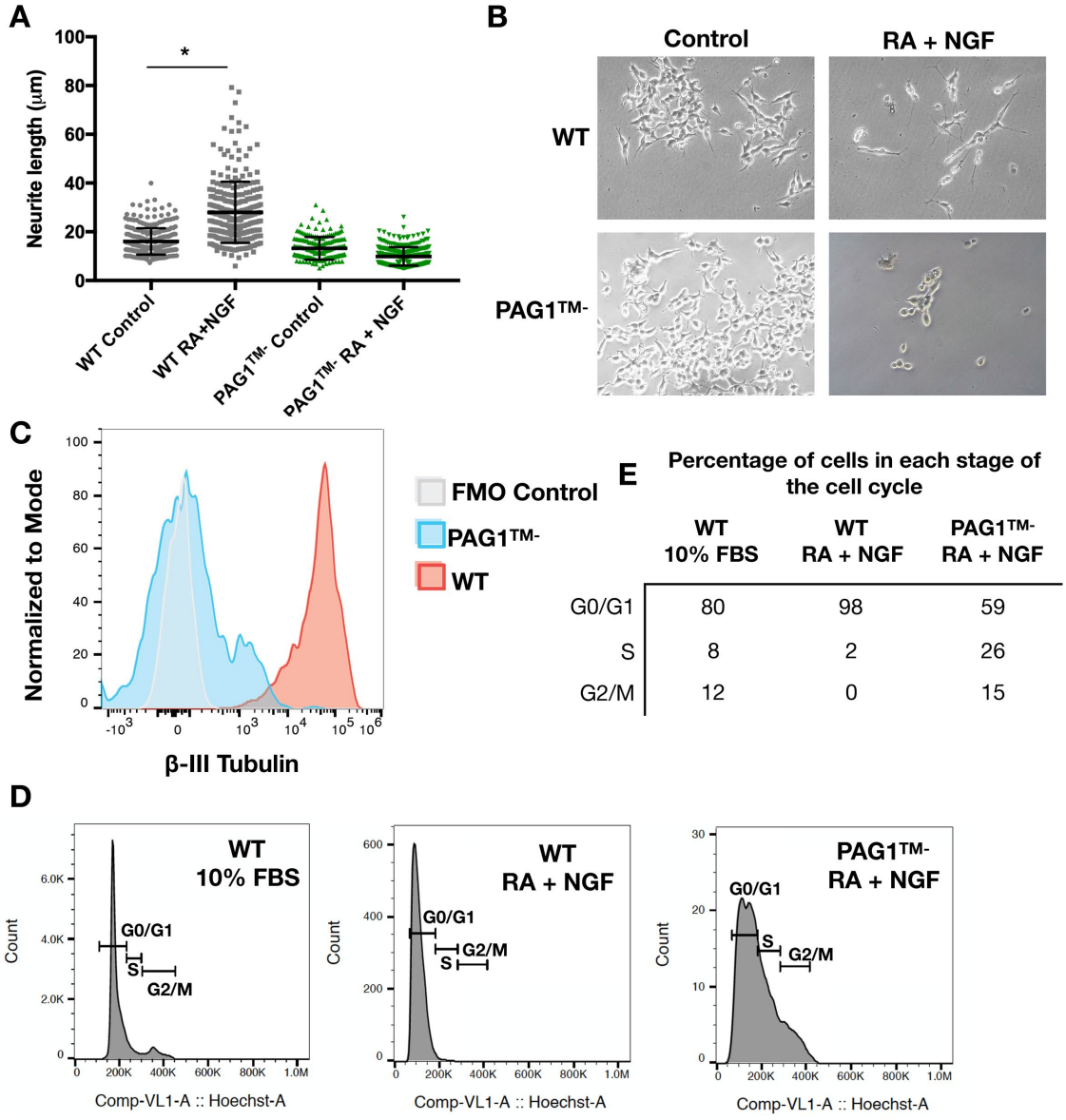

FIGURE 4: PAG1^{TM-} prevented differentiation in SH-SY5Y cells. (A) Neurite lengths of WT and PAG1^{TM-} SH-SY5Y cells after growth in control conditions (RPMI 1640, 2% FBS) and in differentiation conditions (RPMI 1640, 2% FBS, 10 μM RA, 5 nM NGF) *$p < 0.05$, $n = 3$. (B) Representative images of neurites after 8 d of growth are in the indicated conditions, 20× magnification. (C) Flow cytometry of β-III tubulin expression, a marker of neuronal differentiation. (D) Cell cycle analysis of WT SH-SY5Y and SH-SY5Y PAG1^{TM-} cells by flow cytometry. Cells were seeded in standard growth medium (RPMI 1640, 10% FBS) on collagen-coated plates and were exposed for 96 h to 10 μm RA and 5 nM NGF in low serum media (2% FBS). Cells were then stained with Hoechst 33342 and relative DNA content was measured by flow cytometry. (E) The percentage of cells in each stage of the cell cycle for each condition in D. (Results in B–D are representative of at least three independent experiments.)

neuroblastoma cells after 5- and 60-min stimulations with different RTK ligands.

While activation of EGFR induced a robust pERK response in both cell types, PAG1^{TM-} cells had significantly more activated ERK, especially after 5 and 60 min of EGF stimulation (Figure 5, A and B). Treatment with EGF caused a modest increase in pSFK activation in WT cells after both 5 and 60 min (Figure 5, C and D). PAG1^{TM-} cells started at a higher baseline of pSFK activation (Figure 1E), and there was no further increase in the amount of active SFKs after exposure to EGF. These results suggest that PAG1^{TM-} cells retained their ability to activate the RAS/MAPK cell signaling pathway in response to EGF despite a high baseline of activated SFKs.

PAG1^{TM-} increased SRC activation in response to SCF

We then asked if the signaling responses observed after EGFR stimulation were similar to those of another typically pro-oncogenic receptor, KIT. We had previously shown that KIT stimulation by SCF caused an increase of SFKs in endosomes in LAN-6 neuroblastoma cells (Palacios-Moreno *et al.*, 2015), so we asked whether expression of PAG1^{TM-} would affect ERK and SFK responses. KIT activation did not induce a pERK response in either WT or PAG1^{TM-} cells (Figure 6, A and B). However, SCF treatment did increase total pSFK levels at 5 min in both cell types (Figure 6, C and D). As noted above, PAG1^{TM-} cells started at higher basal levels of pSFK activation, but with SCF the amount of pSFKs increased further on ligand

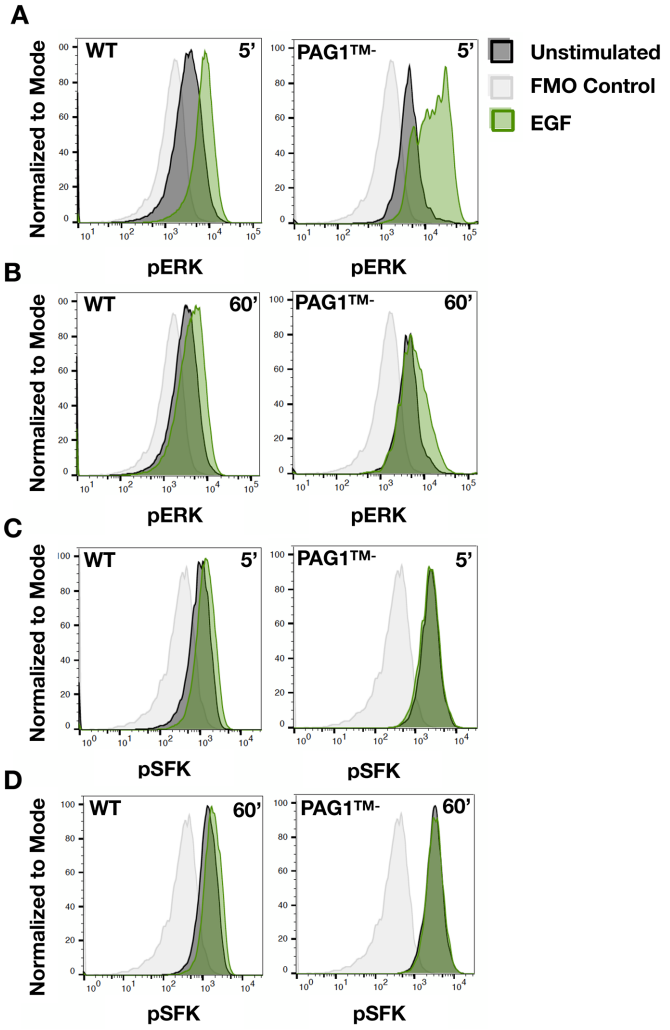

FIGURE 5: PAG1^{TM-} enhanced the pERK response to EGF. Flow cytometry analysis of pERK (A, B) and pSFK (C, D) activation after exposure to 5 nM EGF for either 5 min (A and C) or 60 min (B and D). Adherent SH-SY5Y cells expressing either WT PAG1 or PAG1^{TM-} were treated with ligand before fixing and staining with fluorescent antibodies for pERK (Phospho-p44/42 MAPK [Erk1/2] [Thr202/Tyr204]) and pSFKs (pY416). Data displayed are from one experiment representative of at least three independent experiments. Cell counts were normalized to mode to account for differences in final cell number.

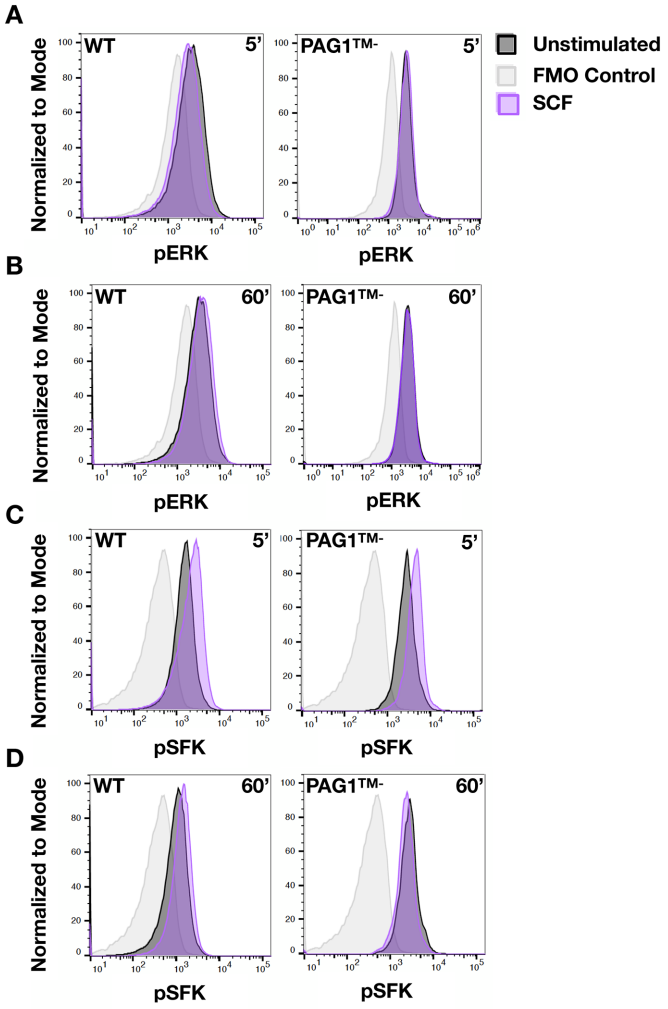

FIGURE 6: PAG1^{TM-} increased SRC response to KIT activation. Flow cytometry analysis of pERK and pSFK activation as in Figure 5 except cells were exposed to 5 nM SCF for either 5 or 60 min. Data displayed are from one experiment representative of at least three independent experiments.

stimulation, mainly at 5 min. WT cells started at a low level of pSFK activation but exhibited a similar increase in pSFK levels on ligand stimulation. These results show that PAG1^{TM-} cells retain the ability to respond to SCF by further increasing SFK activation.

PAG1^{TM-} abrogated ERK activation in response to NGF and GDNF

That PAG1^{TM-} cells failed to differentiate (Figure 4) suggests that cell signaling mechanisms activated in response to RTKs that induce neuronal differentiation may be impaired. Stimulation of TRKA (NTRK1) and RET by NGF and GDNF, respectively, is known to induce differentiation and survival in neurons and neuroblastoma cells (Miller and Kaplan, 2001; Harrington *et al.*, 2011). While WT cells exhibited a robust increase in pERK in response to NGF, the pERK response was entirely absent in PAG1^{TM-} cells (Figure 7, A and B). TRKA activation did lead to small increases in pSFK activation in both WT and PAG1^{TM-} cells; however, this response was short-lived and largely gone by 60 min (Figure 7, C and D). Activation of RET by GDNF induced similar pERK responses in WT, but not PAG1^{TM-} cells, and GDNF induced a more robust early pSFK stimulation in WT but not PAG1^{TM-} cells (Supplemental Figure S1). These results show that PAG1^{TM-} cells are unable to activate the RAS/MAPK pathway in response to two different RTKs that promote neuronal differentiation.

The AKT/PI3K pathway is also activated by RTK signaling; however, we did not detect any changes in AKT phosphorylation that were not associated with the G2/M stage of the cell cycle (Supplemental Figure S2A). PAG1^{TM-} cells had a higher growth rate (Figure 2) and greater percentage of cells in G2/M, which likely explains a greater percentage of cells with high pAKT (pT308) compared with WT cells (Supplemental Figure S2B).

These results distinguish downstream cell signaling responses to different RTKs and indicate that PAG1 is necessary for cells to respond to RTKs that promote neuronal differentiation. Responses to proliferative signals remained intact in the presence of cytoplasmic-truncated PAG1^{TM-}, which we hypothesize acts as a dominant negative by binding regulatory proteins such as CSK in the cytosol and keeping them from interacting with SFKs on membranes. In the

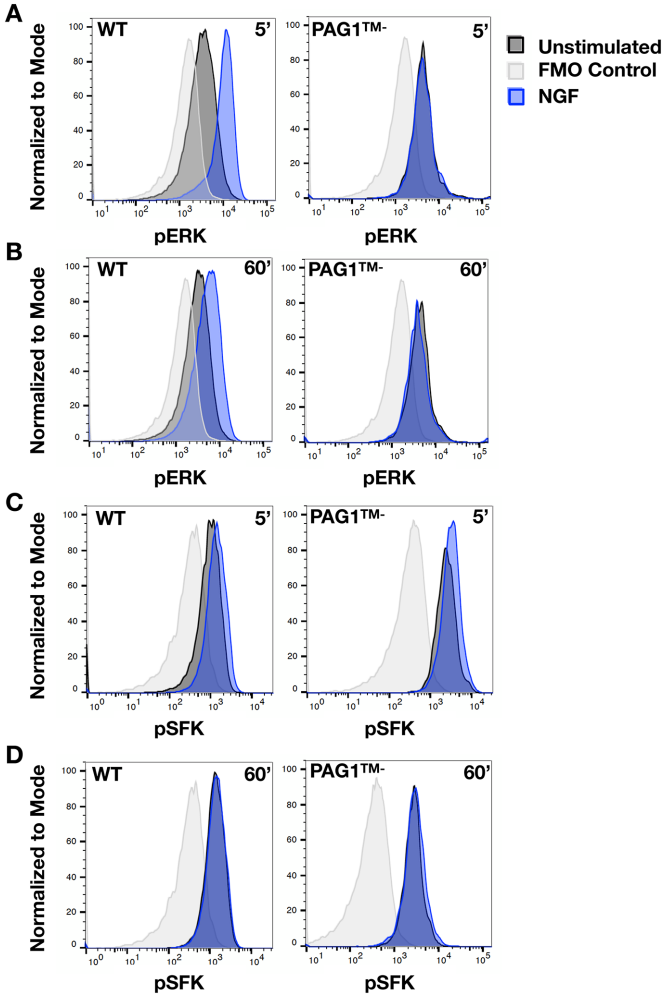

FIGURE 7: PAG1^{TM-} decreased responses to pro-differentiation receptor TRKA. Flow cytometry analysis of pERK and pSFK activation as in Figure 5 except cells were exposed to 5 nM NGF for either 5 or 60 min. Data displayed are from one experiment representative of at least three independent experiments.

canonical view, KIT, EGFR, NGF, and RET should all activate the RAS/MAPK and SFK pathways in response to ligand, yet these receptors produce different responses. Our results so far suggest that there is an additional layer of regulation between receptor activation and ERK/SFK activation. We hypothesized that PAG1's role is to control the activity and intracellular localization of members of the SFK family. We focus on FYN and LYN because of their robust expression in neuroblastoma cell lines and dynamic localization to endosomes and other cell membranes (Palacios-Moreno *et al.*, 2015).

PAG1^{TM-} expression altered FYN and LYN distribution in endosomes

Because PAG1 was detected in endosomes with FYN and LYN (Palacios-Moreno *et al.*, 2015), we hypothesized that PAG1^{TM-} expression may affect the endosomal localization of FYN and LYN. To determine SFK localization in WT and PAG1^{TM-}-expressing cells, we performed organelle fractionation experiments to isolate endosomes as previously described (McCaffrey *et al.*, 2009; Palacios-Moreno *et al.*, 2015). Under conditions of serum starvation, the distribution of FYN and LYN in endocytic organelles was distinct in both PAG1^{TM-} and WT cells (Supplemental Figure S3), consistent with data from LAN-6 neuroblastoma cells (Palacios-Moreno *et al.*, 2015). When KIT was activated by SCF, more FYN and LYN were detected in endosomal fractions of PAG1^{TM-} cells. These effects were similar to those observed previously, though ligand-induced redistribution of FYN and LYN was not as dramatic as in LAN-6 cells (Palacios-Moreno *et al.*, 2015).

FYN and LYN were sequestered in the lumen of MVBs, and their sequestration was affected by PAG1^{TM-} expression

Taelman *et al.* (2010) first reported sequestration of the kinase GSK3β in intraluminal vesicles of MVBs as a means of controlling kinase access to cytoplasmic substrates (Taelman *et al.*, 2010; Vinyoles *et al.*, 2014). We hypothesized that PAG1^{TM-} may regulate FYN and LYN access to cytosolic substrates by sequestration into MVBs in a similar manner. To test this, we isolated endosome fractions via organelle fractionation and performed a protease protection assay. To examine the effects of proliferative signals, cells were either grown in 10% fetal bovine serum (FBS) containing medium (+serum) or serum starved (–serum) for 2 h.

After 30 min of treatment with Protease K, both FYN and LYN were protected in endosome fractions, but degraded in the presence of detergent, indicating that these proteins reside in the lumen of membrane-enclosed organelles such as MVBs (Figure 8A). The lower molecular weight isoform of FYN, FYN isoform C, was preferentially protected (Figure 8A, <60-kD band). Transferrin receptor (TfR), a marker of recycling endosomes, exhibited minimal protection after 5 min of incubation with protease and was not protected after 30 min of protease treatment, as expected for a protein that is not in the lumen of MVBs. We also detected FYN and LYN (but not TfR) in exosomes isolated from WT and PAG1^{TM-} cell culture media (Figure 8B). These data strongly suggest that localization of both FYN and LYN in the lumen of MVBs is a means to control their activity by limiting access to cytosolic substrates.

There were several differences between WT and PAG1^{TM-} cells. First, there was more total FYN and (to a lesser extent) LYN sequestered in the lumen of MVBs from PAG1^{TM-} cells, indicated by protease protection and presence in exosomes (Figure 8). Similar amounts of endosomes were recovered from each cell type in these experiments indicated by TfR (Figures 8A and 9A, TfR). Second, while the amounts of activated SFKs protected from protease were somewhat similar, WT cells had several pSFKs, whereas PAG1^{TM-} cells predominantly had a single activated SFK (pSFK, Figure 8A). Comparing pSFKs to total FYN and LYN, the data indicate that WT cells preferentially sequestered activated SFKs, and PAG1^{TM-} cells sequestered more total FYN and LYN (so the ratio of active to total SFKs was lower). FYN was predominantly recovered by immunoprecipitation (IP) with anti-pSFK antibodies in endosome fractions in PAG1^{TM-} cells (Figure 9A), indicating that the single pSFK band in PAG1^{TM-} cells in Figure 8A is FYN. Much less LYN was recovered by IP from PAG1^{TM-} endosomes (Figure 9A).

There was dramatically more FYN, and activated FYN recovered by pSFK IP, in PAG1^{TM-} endosomes in serum-free conditions compared with +serum (Figure 9A, FYN, pSFK). In WT cells, with serum, there were lower amounts of sequestered total FYN and LYN and active SFKs (Figure 8A). The data suggest that with low growth factor signaling (–serum) active SFKs were sequestered in MVBs and thus separated from interacting proteins in the cytosol (Figure 8A). In cells lacking functional PAG1, this pattern was disrupted, and both active and inactive SFKs were sequestered in MVBs. SFKs were constitutively active in PAG1^{TM-} cells in serum-starved conditions (Figure 1E), and more were detected in MVBs (Figures 8 and 9).

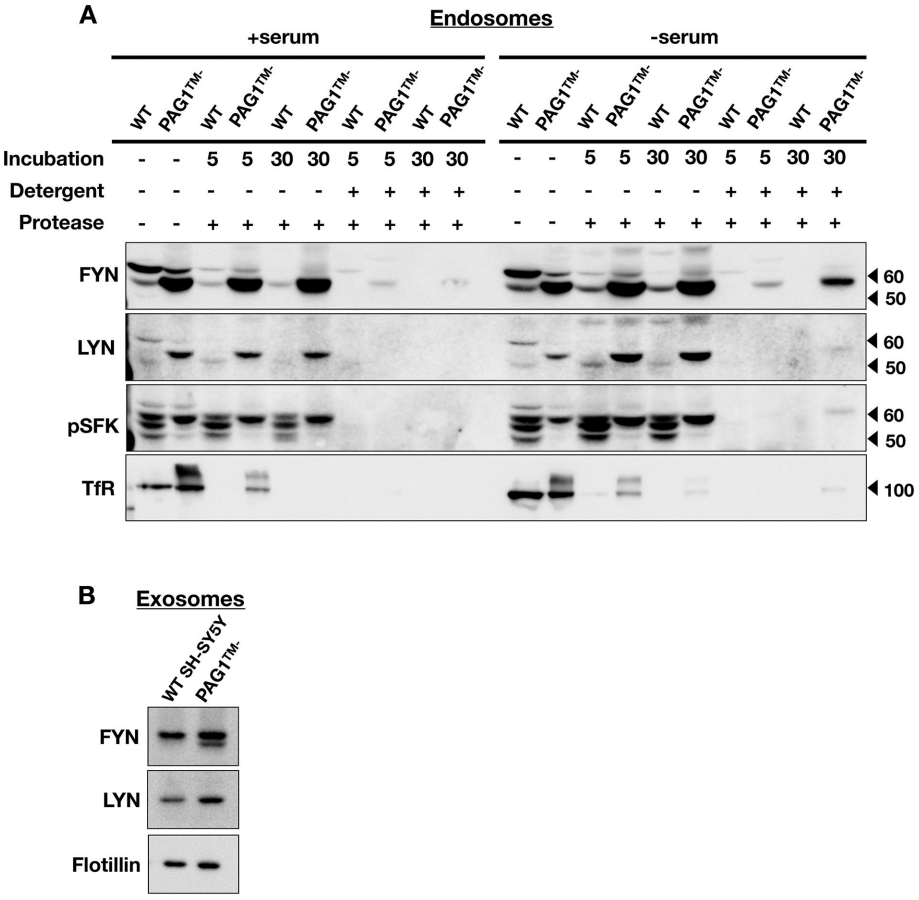

FIGURE 8: WT and PAG1^{TM-} SH-SY5Ys sequestered active SFKs in MVBs. (A) SH-SY5Y cells expressing either WT PAG1 or PAG1^{TM-} were grown in either 10% FBS containing medium (+serum) or serum starved (–serum) before cellular fractionation. The endosome fraction was equally distributed into five parts before treatment with the indicated combinations of detergent (0.1% IGEPAL) and/or Protease K (0.01 μg/μl). Treatments were incubated for 5 min (5) or 30 min (30) at 37°C and stopped by TCA addition. TfR, a marker for recycling endosomes, was used as a negative control for sequestration. (B) Exosomes isolated from WT SH-SY5Y or PAG1^{TM-} SH-SY5Y growth mediums. Western blots show FYN, LYN, and flotillin in exosomes; we detected no TfR in exosomes (unpublished data). Results are representative of at least three independent experiments.

Together, the data suggest that sequestration into the lumen of MVBs is a newly identified mechanism to control SFK activity. It was previously known that PAG1 regulates SFK activity by serving as a scaffold to bring SFKs together with proteins that regulate them (e.g., CSK) (Oneyama *et al.*, 2008). Our data suggest that PAG1 also directs SFK localization to the plasma membrane or endosomes depending on growth factor signaling. Furthermore, the selective ablation of signals that induce differentiation (NGF, GDNF; Figure 7 and Supplemental Figure S1) but not proliferation (EGF; Figure 5) caused by expression of a truncated PAG1 suggests that this mechanism is responsible for distinguishing responses to different RTKs.

DISCUSSION

We had previously shown that the SFKs, FYN and LYN, changed intracellular location in endosomes and lipid rafts in response to stimulation of different RTKs (Palacios-Moreno *et al.*, 2015). In addition, phosphoproteomics identified that the SFK scaffold protein, PAG1, enriched and highly phosphorylated in endosomes and lipid rafts, frequently colocalized with FYN and LYN in neuroblastoma cells (Palacios-Moreno *et al.*, 2015). Specifically, signaling by the receptors ALK and KIT increased the amount of FYN and LYN in cellular fractions containing late endosomes and MVBs. In contrast, signaling by TRKA and RET, two receptors known to induce neuronal differentiation in sympathoadrenal neural crest lineages and neuroblastoma cell lines, shifted FYN and LYN from late endosome/MVB fractions to plasma membrane lipid rafts (Palacios-Moreno *et al.*, 2015). We hypothesized that PAG1 may play a role in this shiftable localization of SFKs in response to RTKs to control downstream cell signaling effectors and responses. Here we demonstrated that expression of PAG1 lacking the transmembrane domain (PAG1^{TM-}) changed SFK activity and localization and abrogated cell differentiation signals but left proliferation signals intact.

Textbooks present the simplified view that RTKs all activate the same four canonical intracellular signaling pathways (RAS/ERK, PLC-γ, SFK, and PI3K/AKT), yet some RTKs cause proliferation and others differentiation. Marshall (1995) proposed that sustained ERK signaling is required for differentiation. Chen *et al.* (2012b) described a gradient of ERK versus AKT activation that controls PC12 cell responses to NGF. In the latter model, higher levels of AKT activation lead to increased cell proliferation while higher levels of ERK activation lead to cell differentiation or lower rates of proliferation. Our data address cell signaling events that likely control ERK and AKT responses; we found that directed localization of SFKs to plasma membrane versus the lumen of MVBs is an important mechanism to control differentiation. Sequestration in MVBs in PAG1^{TM-} cells likely abrogates SFK activation at the plasma membrane in response to differentiation signals and therefore decreases subsequent cellular responses such as ERK activation (Figure 7 and Supplemental Figure S1) and extension of neurites (Figure 4). We hypothesize that PAG1^{TM-} acts as a dominant negative by binding CSK and other cytoplasmic SFK-interacting proteins, which may explain why the effect on differentiation we observe is stronger than that seen in PAG1 knockout mice (Lindquist *et al.*, 2011). Conversely, an increase of active FYN and LYN in endosomes enhanced responses to EGFR and KIT receptors (Figures 5 and 6) and led to an increase in growth rate and anchorage-independent growth in PAG1^{TM-} cells (Figures 2 and 3). Thus, our results suggest that precise spatiotemporal regulation of SFK activity distinguishes RTKs that promote differentiation from those that promote proliferation, and that PAG1 plays a role in this process, which extends the model that defines RTK signals for differentiation (Marshall, 1995; Chen *et al.*, 2012b).

PAG1^{TM-} cells exhibited increased proliferation (Figure 2) and increased the number of cells in the S and G2/M stages of the cell cycle under differentiation conditions (Figure 4). In agreement with previous work showing that AKT activation occurs predominantly after DNA replication in G2/M stages of the cell cycle (Liu *et al.*, 2014), we found that cells with high levels of pAKT were correlated

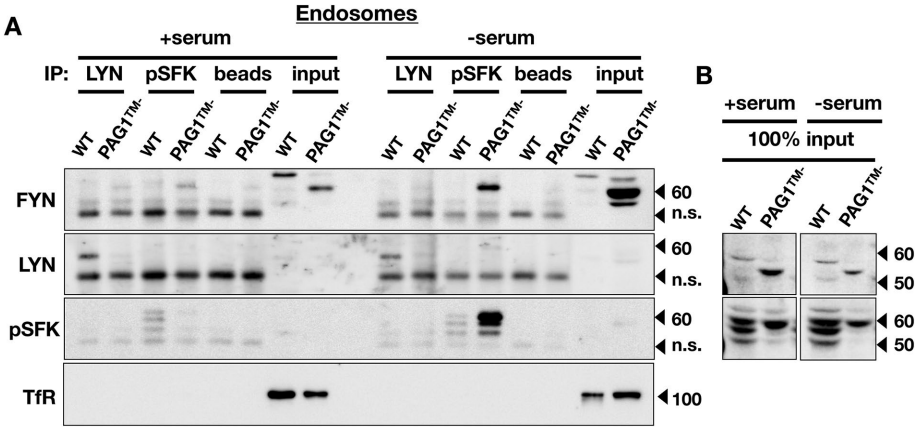

FIGURE 9: FYN was the major active SFK in PAG1^{TM-} SH-SY5Y cells. LYN and pSFKs (Y416) were immunoprecipitated (IP) from endosome fractions of WT and PAG1^{TM-} SH-SY5Y cells grown in either 10% FBS containing medium (+serum) or serum starved (–serum). Fractions were equally distributed into four parts for IPs. Samples were run on SDS–PAGE and the membrane was probed for LYN, FYN, pSFK (Y416), and TfR. In PAG1^{TM-} cells, there was about fourfold increase in FYN immunoprecipitated by pSFK IP comparing –serum endosomes to +serum, and the pSFK signal increased 75-fold, whereas in WT cells, there was a 40% decrease in pSFK and very little FYN was detected. Input in A is 1/20th of the total sample. (B) Input from Figure 8 blots (same experiment) to show LYN and pSFK input amounts; n.s., nonspecific band. Results are representative of at least three independent experiments.

with the number of cells in the G2/M stages of the cell cycle for both PAG1^{TM-} and WT cells (Supplemental Figure S2). This explains why we detected less pAKT in neuroblastoma cells under long-term differentiation conditions where cell division was reduced (unpublished results). The pAKT response to EGF is more rapid than the pERK response, peaking at about 3 min (Zheng *et al.*, 2013), which likely explains why significant changes in AKT activation in response to ligands at 5 and 60 min as for pERK (Figures 5–7) were difficult to detect using flow cytometry methods used here. PI3K and AKT signaling are important for coordinating proliferative growth factor signaling and metabolism (Manning and Toker, 2017; Bilanges *et al.*, 2019), yet it may be that only low levels of AKT activity are required for neuronal differentiation. Nevertheless, given the interconnected nature of cell signaling pathways (Zheng *et al.*, 2013; Grimes *et al.*, 2018), we can predict coordination with other signaling pathways downstream of RTK activation during differentiation, such as PLC-γ, PI3K, AKT, and mTOR complexes, which are also involved in endocytic trafficking and lysosomal degradation (Manning and Toker, 2017; Bilanges *et al.*, 2019). In any case, our results support a role for SFKs, namely FYN and LYN, and control of their activity and intracellular localization by PAG1, as a mechanism to distinguish differentiation signals caused by the RTKs TRKA and RET.

A defect in differentiation, together with increased activity of total SFKs we observed in cells expressing PAG1^{TM-} (Figure 1), is consistent with previous observations that PAG1 acts as a tumor suppressor in neuroblastoma cells (Oneyama *et al.*, 2008; Agarwal *et al.*, 2016). Oneyama *et al.* (2008) first demonstrated the interaction between PAG1 and SRC. They found that PAG1 mediates the inhibitory C-terminal phosphorylation of SFKs via binding CSK, and that a lipid–raft-anchored SRC variant was largely inactive. Consistent with our soft agar assay data (Figure 3), cells lacking PAG1 formed almost 20 times as many colonies as those re-expressing functional PAG1 in colony transformation assays (Oneyama *et al.*, 2008). Using siRNA knockdown of PAG1, Agarwal *et al.* (2016) also demonstrated increased SFK activity, increased anchorage-independent growth, and increased ERK activity in neuroblastoma cell lines (Agarwal *et al.*, 2016). A PAG1 mutant that lacked residues required for lipid raft localization failed to suppress SRC-mediated transformation (Oneyama *et al.*, 2008), which emphasizes the importance of membrane localization of PAG1 for regulation of SFK activity. These data are consistent with our results with a PAG1 mutant lacking the transmembrane domain. Together, these studies suggest that defects in PAG1, whether through mutation or change in protein amount, have pro-proliferative effects and solidify its role as a tumor suppressor.

Sequestration of active SFKs into MVBs represents a previously unappreciated method by which cells control SFK activity (Figure 8). FYN and LYN have been seen in structures that appear to be endosomes by fluorescence microscopy (Donepudi and Resh, 2008), and previous work showing SRC trafficking to, and regulating several components of, the endo/lysosomal pathway predicts that they should be found in MVBs (Reinecke and Caplan, 2014). Our studies suggest that MVB sequestration regulates SFK kinase activity toward cytosolic substrates similar to GSK3β kinase sequestration in the WNT signaling pathway (Taelman *et al.*, 2010; Vinyoles *et al.*, 2014). The data suggest that in the absence of signaling, such as during serum starvation, active SFKs are sequestered in MVBs, and RTKs, especially those that induce differentiation, keep SFKs active at the plasma membrane in lipid rafts. This mechanism was disrupted in PAG1^{TM-} cells, which sequestered large amounts of total FYN and LYN (Figure 8). Interestingly, only FYN was immunoprecipitated by anti-phospho-SFK antibodies in endosome fractions, and activated FYN dramatically increased in MVBs under serum starvation conditions (Figure 9). In contrast, LYN was not immunoprecipitated by anti-phospho-SFK antibodies in endosomal fractions (Figure 9). This implicates sequestration of active FYN as the primary defect that abrogates the differentiation response. Sequestration of active FYN apparently had no inhibitory effect on growth rate or colony formation, which explains insensitivity to PP2 in PAG1^{TM-} cells (Figures 2 and 3), since PP2 inhibits FYN more effectively than SRC and LYN (Hanke *et al.*, 1996; Brandvold *et al.*, 2012).

We previously identified a potentially antagonistic relationship between FYN and LYN activation using computational analysis to identify patterns in phosphoproteomic data (Palacios-Moreno *et al.*, 2015). In many neuroblastoma cell lines, activated FYN (pY420) was frequently associated with inhibited LYN (pY508), and in other cases, inhibited FYN (pY531) was frequently associated with several phosphorylations on PAG1 (Palacios-Moreno *et al.*, 2015). These data suggest that an antagonistic relationship between FYN and LYN activation, potentially mediated by an inhibitory interaction between PAG1 and FYN, may be part of the cell signaling network that distinguishes RTK signals that promode differentiation, proliferation, or other cell responses.

Sequestration into MVBs may simply lead to protein degradation in the lysosome (Lys); however, there appear to be different populations of MVBs with longer half-lives, which may give rise to additional signaling functions (Huotari and Helenius, 2011). Receptor signaling from endosomal membranes after endocytosis influences temporal and spatial regulation of signaling effector pathways

downstream from receptor activation (Irannejad *et al.*, 2015; Bergeron *et al.*, 2016). The presence of activated FYN in the lumen of MVBs, together with its role in neuronal differentiation noted above, suggests that FYN is potentially another important component of signaling endosomes in neurons, which play an important role in nervous system development and neurodegenerative disease (Harrington and Ginty, 2013; Cosker and Segal, 2014; Marlin and Li, 2015; Bergeron *et al.*, 2016; Scott-Solomon and Kuruvilla, 2018; Chen and Mobley, 2019). Signaling endosomes containing NGF and TRKA have been identified in neurons to be Rab7-positive MVBs (Von Bartheld and Altick, 2011; Harrington and Ginty, 2013). Back fusion of luminal vesicles from MVBs would release active FYN and other kinases identified in signaling endosomes into neuronal cell bodies after retrograde transport (Von Bartheld and Altick, 2011; Falguières *et al.*, 2012; Bissig and Gruenberg, 2014; Ye *et al.*, 2018). Strong evidence for this was obtained by Ye *et al.* (2018), who showed that TRKA-containing MVBs are retrogradely transported in neurons and persist in the cell body, where TRKA is then re-expressed on the surface of endosomes and thus has access to cytosolic substrates (Ye *et al.*, 2018). Further work will be necessary to determine whether FYN (and other SFKs) are retrogradely transported in the lumen of axonal MVBs and subsequently released into neuronal cell bodies.

MVBs can also fuse with the plasma membrane and release intraluminal vesicles as exosomes. Exosomes containing Wnt10b promote axon regeneration after neural injury (Tassew *et al.*, 2017), and it is possible that "signaling exosomes" also play a role in nervous system development. We detected FYN and LYN in exosomes isolated from WT and PAG1^{TM-} cell culture media (Figure 8B). Release of active FYN and LYN in exosomes, which can bind and signal to neighboring cells, may be one method by which global pSFK signals are increased in PAG1^{TM-} cells (Figure 1). In accordance with this idea, more FYN was detected in PAG1^{TM-} exosomes, and more FYN was immunoprecipitated with pSFK in endosomes (Figures 8 and 9).

In conclusion, the data presented here further support a role for PAG1 as a key integrator of RTK signaling downstream of receptor activation and support its previously identified role as a tumor suppressor. Our data, together with our previous findings (Palacios-Moreno *et al.*, 2015), fit with a model where PAG1 directs SFK intracellular localization to plasma membrane or endosomal compartments depending on the particular receptor activated by its ligand. PAG1 thus connects upstream RTK signals to SFKs, which in turn control other downstream effectors to induce cell differentiation. Furthermore, we demonstrate a new mechanism for regulation of SFK activity: sequestration into MVBs, which impacts many aspects of SFK signaling. These results support the broad hypothesis that the spatial regulation of pathways downstream of RTK activation within endosomes is a key mechanism by which cells determine a response to extracellular signals (Bergeron *et al.*, 2016).

MATERIALS AND METHODS

Cell culture

SH-SY5Y neuroblastoma cell lines were cultured in RPMI 1640 medium (Thermo Scientific HyClone, USA) supplemented with sodium bicarbonate (Sigma, USA) and 10% FBS (Corning). Cells were maintained in a humidified incubator at 37°C, 5% CO_2.

CRISPR/Cas9 targeting of PAG1

CRISPR/Cas9 plasmids and sgRNAs targeting Exon 5 and 7 of the PAG1 gene were provided by Blake Wiedenheft and Royce Wilkinson (Montana State University). sgRNA sequences were housed in the lentiviral Cas9/sgRNA vector (Addgene #57828).

Exon 5 sgRNA: 5′-GAAGCCGCGACAGCATAGTG GGG-3′.
Exon 7 sgRNA: 5′-GCAGATCCGAGGCCGATGTC TGG-3′.

The plasmid carrying Cas9/sgRNA was cotransfected into HEK293FT cells with the lentiviral packaging vectors psPAX2 (Addgene #12260) and VSV-g (Addgene #8454) following the Lipofectamine 3000 protocol (ThermoFisher) to generate lentivirus. Supernatants containing lentivirus were filtered through a low-protein-binding syringe filter (0.45 µm, Millipore #SLHP033RS) before transductions. SH-SY5Y cells were transduced with different dilutions of virus-containing supernatant, and transfected cells were selected for by Puromycin (3 µg/ml) addition to culture media. Pools of puromycin-resistant cells were analyzed by Western blot for PAG1 expression, and those lacking PAG1 were characterized further. DNA surrounding the target site was amplified by PCR; PCR products were sequenced by Eurofins. While PAG1 expression appeared to be ablated in initial screens, we subsequently noted a truncated, soluble protein expressed in these cells (described in *Results*).

Neurite extension

Cells were seeded according to calculated doubling times to control for initial increases in proliferation. WT SH-SY5Y (30,000 cells/well) or PAG1^{TM-} SH-SY5Y (9000 cells/well) cells were seeded in 6-well plates containing RPMI 1640 + 10% FBS. Cells were grown for 2–4 d until fully adhered. Spent media were aspirated and replaced with differentiation media composed of RPMI 1640 + 2% FBS, 10 µM 9-cis-RA (Sigma-Aldrich) and/or 5 nM human β-NGF (Peprotech). Cells were grown in differentiation media for 8 d; treatment media were replaced every other day. On day 8, neurite tracings, length quantifications, and cell body measurements were performed using ImageJ (Rueden *et al.*, 2017). Only neurites longer than one cell body length were quantified to eliminate lamellipodia/filopodia. Representative images were taken on day 8 using a Zeiss Invertoskop light microscope with an Amscope MD500 camera.

Mass spectrometry sample preparation

Tandem liquid chromatography mass spectrometry (LC-MS) with tandem mass tags was performed on SH-SY5Y and PAG1^{TM-} cells as previously described (Grimes *et al.*, 2018). Briefly, cells were washed and harvested in phosphate-buffered saline (PBS) and cell pellets were frozen in liquid nitrogen. Cells were lysed in a 10:1 (vol/wt) volume of lysis buffer (4% SDS; 100 mM NaCl; 20 mM HEPES, pH 8.5; 5 mM dithiothreitol [DTT]; 2.5 mM sodium pyrophosphate; 1 mM β-glycerophosphate; 1 mM Na_3VO_4; 1 µg/ml leupeptin), and proteins were reduced at 60°C for 45 min. Proteins were then alkylated by the addition of 10 mM iodoacetamide (Sigma) for 15 min at room temperature in the dark and methanol/chloroform precipitated. Protein pellets were resuspended in urea lysis buffer (8 M urea; 20 mM HEPES, pH 8.0; 1 mM sodium orthovanadate; 2.5 mM sodium pyrophosphate; 1 mM β-glycerophosphate) and sonicated. Samples were diluted fourfold in 20 mM HEPES, pH 8.5, 1 mM $CaCl_2$, for Lys-C digestion overnight at 37°C, then diluted twofold and trypsin digested 4–6 h at 37°C. Samples were then desalted on a C18 SepPak (Waters), then labeled with isobaric tandem-mass-tag (TMT) reagents (Thermo Fisher Scientific, San Jose, CA) in 20 mM pH 8.5 HEPES with 30% acetonitrile (vol/vol). Samples were then mixed in equimolar ratios, and the ratios were checked via LC-MS analysis on an Orbitrap Fusion Lumos mass spectrometer (Thermo Fisher). The combined sample was then purified on a SepPak and dried in a speed-vac. The combined sample was then resuspended in basic reverse-phase (bRP) buffer A (10 mM NH_4HCO_2, pH 10, 5% ACN) and separated via high pH reverse-phase fractionation on a

Zorbax Extended C18 column (2.1 × 150 mm, 3.5 µm, no. 763750-902, Agilent) with a gradient of 10–40% bRP buffer B (10 mM NH_4HCO_2, pH 10, 90% ACN). Ninety-six fractions were collected, consolidated down to 24 fractions, and desalted with a C18 stop and go extraction tip prior to LC-MS analysis on an Orbitrap Fusion Lumos MS.

LC-MS analysis

Samples were analyzed on an Orbitrap Fusion Lumos mass spectrometer (Thermo Fisher Scientific, San Jose, CA) coupled with a Proxeon EASY-nLC 1200 LC pump (Thermo Fisher Scientific, San Jose, CA). Peptides were separated on a 100-µm inner diameter microcapillary column packed with ~40 cm of Accucore150 resin (2.6 µm, 150 Å, Thermo Fisher Scientific, San Jose, CA). For each analysis, we loaded approximately 1 µg onto the column. Peptides were separated using a 2.5 h gradient of 6–30% acetonitrile in 0.125% formic acid with a flow rate of 550 nL/min. Each analysis used an SPS–MS3-based TMT method (Ting *et al.*, 2011; McAlister *et al.* 2014), which has been shown to reduce ion interference compared with MS2 quantification (Paulo *et al.*, 2016). The scan sequence began with an MS1 spectrum (Orbitrap analysis, resolution 120,000; 350–1400 m/z, automatic gain control (AGC) target 4.0 × 105, maximum injection time 50 ms). Precursors for MS2/MS3 analysis were selected using a Top10 method. MS2 analysis consisted of collision-induced dissociation (quadrupole ion trap; AGC 2.0 × 104; normalized collision energy (NCE) 35; maximum injection time 120 ms). Following acquisition of each MS2 spectrum, we collected an MS3 spectrum using a method in which multiple MS2 fragment ions are captured in the MS3 precursor population using isolation waveforms with multiple frequency notches (McAlister *et al.*, 2014). MS3 precursors were fragmented by HCD and analyzed using the Orbitrap (NCE 65, AGC 3.5 × 105, maximum injection time 150 ms, isolation window 1.2 Th, resolution was 50,000 at 200 Th).

Mass spectrometry data processing

Mass spectra were processed using a Sequest-bast software pipeline (Eng *et al.*, 1994). Samples were searched against a fully tryptic human database, allowing for a static modification of lysine and N-termini with TMT (229.1629 Da) and carbamidomethylation (57.0215 Da) of cysteine, along for variable oxidation (15.9949 Da) of methionine. Searches were performed using a 50-ppm precursor ion tolerance; the product ion tolerance was set to 1.0 Da. Peptide-spectrum matches were adjusted to a 1% false discovery rate (FDR) (Elias and Gygi 2007, Elias and Gygi 2010) and to a final protein-level FDR of <2%. Protein assembly was guided by principles of parsimony to produce the smallest set of proteins necessary to account for all observed peptides (Huttlin *et al.*, 2010). For TMT-based reporter ion quantitation, we extracted the summed signal-to-noise (S/N) ratio for each TMT channel and found the closest matching centroid to the expected mass of the TMT reporter ion. MS3 spectra with TMT reporter ion summed signal-to-noise ratios less than 50 were excluded from quantitation (McAlister *et al.*, 2012).

Organelle fractionations

Cell fractionation experiments were performed using previously established methods (McCaffrey *et al.*, 2009; Pryor *et al.*, 2012; Palacios-Moreno *et al.*, 2015). WT LAN-6 or SH-SY5Y cells expressing either WT PAG1 or $PAG1^{TM-}$ were grown to ~90% confluency and serum starved for 2 h prior to cell harvesting. Cells were then consecutively washed with cold PEE (1 mM EDTA, 1 mM EGTA, in 1× PBS) and PGB (0.1% glucose, 0.1% bovine serum albumin [BSA] in 1× PBS) buffers and resuspended in cold PGB containing the indicated RTK ligands. Cells were rotated with ligand for 1 h at 4°C, washed with PGB, resuspended in cold PGB, and incubated for 1 h at 37°C to permit endosomal trafficking. After internalization, cells were quenched in ice water, washed once each with PEE and Bud Buffer (38 mM aspartic acid, 38 mM glutamic acid, 38 mM gluconic acid, 20 mM MOPS, pH 7.1 at 37°C, 10 mM potassium bicarbonate, 0.5 mM magnesium carbonate, 1 mM EDTA, 1 mM EGTA), and resuspended in Bud Buffer containing protease inhibitors. Cells were then mechanically permeabilized by a single passage through a Balch homogenizer. The "cracked" cells were centrifuged (1000 × *g*, 4°C, 10 min) to separate dense membranous fractions from organelles. The membrane pellet was further separated into detergent-resistant membranes (DRM) and detergent-soluble membranes (P1M) by addition of a mild detergent (0.1% IGEPAL) before centrifugation. The organelle-containing supernatant was layered on top of an iodixanol gradient (2.5–25% Optiprep, Sigma-Aldrich) and spun at 100,000 × *g* to separate Lys, endosomes of high mass and density (E1), endosomes of intermediate mass and density (E2), endosomes of low mass and density (E3), and cytosol fractions. To isolate lipid rafts, an iodixanol gradient (2–30% Optiprep) was layered on top of DRM samples and spun to equilibrium at 100,000 × *g* for 18 h, and floating and nonfloating fractions were collected. Fractions from both types of gradients were taken using a Brandel fractionator. All centrifugations were performed using SW55Ti and MLS50 rotors in a Beckman ultracentrifuge. After fractions were collected from gradients, proteins were purified by trichloroacetic acid (TCA)/acetone precipitation prior to suspension in 7 M Urea sample buffer for loading on SDS–PAGE.

Protease protection assay

Fractions containing MVBs and late endosomes (labeled Endosomes) or early endosomes and cytosol (labeled Cytosol) were collected from organelle gradients after treatment (with or without 2 h serum starvation) according to the fractionation protocol. Bottom and top fractions were thoroughly mixed and divided into five equal volumes. Cold TCA (14%) was immediately added to the control fraction; the other four fractions were incubated at 37°C for either 5 or 30 min with combinations of Proteinase K (0.01 µg/ml, Sigma-Aldrich) and/or IGEPAL (0.1%). Cold TCA (14%) was added after each incubation, and samples were stored at 4°C. Proteins in fractions were concentrated using TCA/acetone precipitation before SDS–PAGE and blotting on nitrocellulose.

IPs

Following the organelle fractionation protocol with or without 2 h serum starvation, cells were washed with cold PEE, suspended in Bud Buffer, and cracked using a Balch homogenizer. Fractions obtained after organelle fractionation were thoroughly mixed and divided into equal volumes before adding beads and/or primary antibody. Primary antibody and 10× Cell Signaling Technology (CST) cell lysis buffer (CST to 1× final concentration) were added to each IP sample. Samples were incubated, rotating, at 4°C overnight. A 10% bead solution (Protein A/G UltraLink Resin, Thermo Fisher #53132) was prepared in block buffer (1× lysis buffer containing 5% BSA). Beads were rotated 1 h at 4°C and washed twice with block. Beads were resuspended in 1 mg/ml BSA in 1× lysis buffer. Bead solution was added to each sample and incubated, rotating, at 4°C for 2 h. After incubation, IP beads were washed four times with 1× lysis buffer containing decreasing amounts of BSA (two washes with 0.25 mg/ml, followed by 0.1 mg/ml, and finally no BSA). Samples were resuspended in 7 M Urea sample buffer with DTT before SDS–PAGE and blotted on nitrocellulose.

Flow cytometry

WT SH-SY5Y and PAG1^{TM-} SH-SY5Y cells were grown to 90% confluency before stimulation with RTK ligands. After seeding, cells were incubated for 24–48 h prior to treatment to allow for attachment to the dish. Cells were harvested and washed with cold 1× PEE buffer before fixing in 4% paraformaldehyde in 1× PBS. After fixing, cells were treated with Benzonase in FACS buffer for 10 min at room temperature (to reduce cell clumping) prior to permeabilization with ice-cold methanol. Samples were then incubated with Hoescht 33342 and/or the indicated fluorescent antibodies. Fluorescence minus one controls were prepared from the control conditions within each experiment. Samples were read on a NxT Acoustic Focusing Cytometer (Life Technologies, Carlsbad, CA) using the Attune NxT Software, v2.4, and the resulting data were analyzed using FlowJo v10.0.

MTT assay

SH-SY5Y WT cells were seeded at 50,000 cells/well and SH-SY5Y PAG1^{TM-} cells were seeded at 5000 cells/well in RPMI 1640 containing 10% FBS in a 96-well plate and allowed to adhere for 24 h. Spent media were aspirated and replaced with 100 µl of treatment media (0–5 µM PP2) and incubated for 48 h before MTT addition. For time zero measurements, spent media were aspirated and media containing 5 mg/ml MTT were added and incubated for 4 h. After incubation, 40% wt/vol SDS in HCl, pH 2, was added to dissolve MTT crystals. Absorbance was read at 570 nm in a VersaMax plate reader (Molecular Devices). Growth rates, defined as the number of doublings per day, were calculated by: $R = [\log_2 (A_t/A_0)]/t$, where A_0 and A_t are absorbance measurements before and after treatment, respectively, and t is the number of days in culture. The GRI was calculated as described by Hafner *et al*. (2016) by the formula: $GRI = 2^{(R'/R)}–1$ where R' is the growth rate of cells under the test condition, and R is the control growth rate. In the case of PAG1^{TM-} GRIs, R and R' are the growth rates of WT and PAG1^{TM-} cells, respectively. For PP2 GRIs, R is the growth rate of cells in vehicle-control medium, and R' is the growth rate of cells in PP2 medium. The resulting GRIs were pooled, and the second and third quartiles were used for analysis by plotting and in Welch's *t* tests. One-sample *t* tests were also calculated for PP2 GRIs to determine the statistical significance of growth rate inhibition (as indicated by deviation from 1). In addition, growth rates from all experiments were pooled, and Welch two-sample *t* test was performed to compare WT and PAG1^{TM-} cells.

Soft agar assays

2-Hydroxyethyl agarose (0.6%) was added to the bottom of each well in a 6-well plate. Plates were incubated at 4°C for 1 h to solidify the agar. After 1 h, plates were incubated at 37°C for 30 min before use. SH-SY5Y WT and SH-SY5Y PAG1^{TM-} cells were diluted to a concentration of 80,000 cells/ml. Prewarmed pipettes were used to mix 3% agarose with growth media containing 10% FBS to a final concentration of 0.3% agarose. SH-SY5Y WT or SH-SY5Y PAG1^{TM-} cells were incubated in the media/agarose solution containing drug (5 µM PP2). The cell-containing solutions were then mixed with 2 ml of 0.6% agarose. The cell-agarose solution was added on top of the first agarose layer and incubated at 4°C for 15 min to solidify the agar. Cells were then incubated at 37°C for 1 wk. After 1 wk, the number of colonies over 70 µm in diameter were counted at 40× magnification. A grid was placed over each well which divided the well into six sections and one field of view was counted for each section. The average number of colonies per well and the average number of colonies per condition (average of three wells) was calculated.

Exosome isolation

Exosomes in Figure 8 were isolated using the ME Kit for Exosome Isolation (New England Peptide). WT SH-SY5Ys or PAG1^{TM-} SH-SY5Ys were serum starved for 16 h before collecting cell culture media to prevent contamination from exosomes in FBS. Ultracentrifugation was also used to verify the presence of LYN and FYN in exosomes. WT SH-SY5Ys or PAG1^{TM-} SH-SY5Ys were serum starved for 16 h. Cell culture media were harvested and centrifugations were performed to eliminate contamination from apoptotic bodies: 2000 × *g*, 20 min, 4°C; 5000 × *g*, 60 min, 4°C. The supernatant was collected and centrifuged at 100,000 × *g*, 90 min, 4°C; the exosome pellet was resuspended in 7 M Urea sample buffer for SDS–PAGE and Western blotting.

Antibodies

Flow cytometry: anti-Human/Mouse phospho-SRC (Y418) PerCP-eFluor 710 (Affymetrix/eBioscience); AF647 Mouse anti-Src (pY418) (BD Biosciences); Hoechst 33342 (CST #4082); β-III tubulin (CST #4466); pAKT-PE (pT308) (BD Biosciences); Rabbit anti- pERK-AF488 (Phospho-p44/42 MAPK [Erk1/2] [Thr202/Tyr204]) (CST #13214); Mouse IgG2b K Isotype Control PerCP-eFluor 710 (Affymetrix/eBioscience); Rabbit IgG Isotype Control AF488 (CST #4340); PE Mouse IgG1, κ Isotype Control (BioLegend #400111); AF647 Mouse IgG1, κ Isotype Control (BioLegend #400135).

Western blots: Fyn Antibody 1:1000 (CST #4023); Lyn Antibody 1:1000 (CST #2796); PAG1 (Csk-binding protein antibody PAG-C1) 1:1000 (ThermoFisher #MA1-19287); Phospho-Src family (Tyr416) 1:1000 (CST #6943/2101); Src 1:1000 (CST #2109); TfR H68.4 1:7500 (ThermoFisher 13-6800); Flotillin 1:1000 (CST #3253); ECL Anti-Mouse IgG HRP linked secondary 1:5000 (GE Healthcare #NA931); ECL Anti-Rabbit IgG HRP linked secondary 1:5000 (GE Healthcare #NA934).

Ligands and inhibitors

PP2 (Calbiochem #529573); 9-cis-RA (Sigma Aldrich # R4643); EGF – 5 nM (PeproTech #AF-100-15) (R&D #236-EG-200); GDNF (PeproTech #450-10) (R&D #212-GD-010); β-NGF (PeproTech #450-01) (R&D #256-GF-100); SCF (PeproTech #300-07) (R&D #255-SC-200); PTN (R&D #252-PL).

ACKNOWLEDGMENTS

We gratefully acknowledge Scott Wetzel and Pam Shaw for help with flow cytometry. MM, JD, and JS were supported by the UM Neuroscience summer research program with the assistance of funding from the WM Keck Foundation. This work was supported by National Institutes of Health (NIH) DE028434-01A, NIH NS070746-01, NS061303-01, COBRE National Center for Research Resources (NCRR) Grant P20 RR015583, and generous donations from Craig Wilkinson. L.F. was supported by Centers of Biomedical Research Excellence (COBRE) NCRR Grant P20GM103546.

REFERENCES

Agarwal S, Ghosh R, Chen Z, Lakoma A, Gunaratne PH, Kim ES, Shohet JM (2016). Transmembrane adaptor protein PAG1 is a novel tumor suppressor in neuroblastoma. Oncotarget 5, 1–9.

Alland L, Peseckis SM, Atherton RE, Berthiaume L, Resh MD (1994). Dual myristylation and palmitylation of Src family member p59fyn affects subcellular localization. J Biol Chem 269, 16701–16705.

Barua D, Hlavacek WS, Lipniacki T (2012). A computational model for early events in B cell antigen receptor signaling: analysis of the roles of Lyn and Fyn. J Immunol 189, 646–658.

Bergeron JJM, Di Guglielmo GM, Dahan S, Dominguez M, Posner BI (2016). Spatial and temporal regulation of receptor tyrosine kinase activation and intracellular signal transduction. Annu Rev Biochem 14, 1–25.

Bilanges B, Posor Y, Vanhaesebroeck B (2019). PI3K isoforms in cell signalling and vesicle trafficking. Nat Rev Mol Cell Biol 20, 515–534.
Bissig C, Gruenberg J (2014). ALIX and the multivesicular endosome: ALIX in Wonderland. Trends Cell Biol 24, 19–25.
Brandvold KR, Steffey ME, Fox CC, Soellner MB (2012). Development of a highly selective c-Src kinase inhibitor. ACS Chem Biol 7, 1393–1398.
Chen J, McKay RM, Parada LF (2012a). Malignant glioma: Lessons from genomics, mouse models, and stem cells. Cell 149, 36–47.
Chen JY, Lin JR, Cimprich KA, Meyer T (2012b). A Two-Dimensional ERK-AKT Signaling Code for an NGF-Triggered Cell-Fate Decision. Mol Cell 45, 196–209.
Chen XQ, Mobley WC (2019). Exploring the pathogenesis of Alzheimer disease in basal forebrain cholinergic neurons: Converging insights from alternative hypotheses. Front Neurosci 13, 446.
Cosker KE, Segal RA (2014). Neuronal signaling through endocytosis. Cold Spring Harb Perspect Biol 6, a020669.
Donepudi M, Resh MD (2008). c-Src trafficking and co-localization with the EGF receptor promotes EGF ligand-independent EGF receptor activation and signaling. Cell Signal 20, 1359–1367.
Elias JE, Gygi SP (2007). Target-decoy search strategy for increased confidence in large-scale protein identifications by mass spectrometry. Nat Methods 4, 207–214.
Elias JE, Gygi SP (2010). An overview of label-free quantitation methods in proteomics by mass spectrometry. Methods Mol Biol 604, 55–71.
Falguières T, Castle D, Gruenberg J (2012). Regulation of the MVB Pathway by SCAMP3. Traffic 13, 131–142.
Eng JK, McCormack AL, Yates JR (1994). An approach to correlate tandem mass spectral data of peptides with amino acid sequences in a protein database. J Am Soc Mass Spectrom 5, 976–989.
Grimes M, Hall B, Foltz L, Levy T, Rikova K, Gaiser J, Cook W, Smirnova E, Wheeler T, Clark NR, *et al.* (2018). Integration of protein phosphorylation, acetylation, and methylation data sets to outline lung cancer signaling networks. Sci Signal 11, 1–16.
Guo J, Walss-Bass C, Luduena RF (2010). The Beta isotypes of tubulin in neuronal differentiation. Cytoskeleton 67, 431–441.
Hafner M, Niepel M, Chung M, Sorger PK (2016). Growth rate inhibition metrics correct for confounders in measuring sensitivity to cancer drugs. Nat Methods 13, 521–527.
Hanke JH, Gardner JP, Dow RL, Changelian PS, Brissette WH, Weringer EJ, Pollok BA, Connelly PA (1996). Discovery of a novel, potent, and Src family-selective tyrosine kinase inhibitor. J Biol Chem 271, 695–701.
Hantschel O, Nagar B, Guettler S, Kretzschmar J, Dorey K, Kuriyan J, Superti-Furga G (2003). A myristoyl/phosphotyrosine switch regulates c-Abl. Cell 112, 845–857.
Harrington AW, Ginty DD (2013). Long-distance retrograde neurotrophic factor signalling in neurons. Nat Rev Neurosci 14, 177–187.
Harrington AW, St. Hillaire C, Zweifel LS, Glebova NO, Philippidou P, Halegoua S, Ginty DD (2011). Recruitment of actin modifiers to TrkA endosomes governs retrograde NGF signaling and survival. Cell 146, 421–434.
Harrison SC (2003). Variation on an Src-like theme. Cell 112, 737–740.
Huotari J, Helenius A (2011). Endosome maturation. EMBO J 30, 3481–3500.
Iglesias-Bartolome R, Gutkind JS (2011). Signaling circuitries controlling stem cell fate: To be or not to be. Curr Opin Cell Biol 23, 716–723.
Huttlin EL, *et al.* (2010). A tissue-specific atlas of mouse protein phosphorylation and expression. Cell 143, 1174–1189.
Ingley E, Schneider JR, Payne CJ, McCarthy DJ, Harder KW, Hibbs ML, Klinken SP (2006). Csk-binding protein mediates sequential enzymatic down-regulation and degradation of Lyn in erythropoietin-stimulated cells. J Biol Chem 281, 31920–31929.
Irannejad R, Tsvetanova NG, Lobingier BT, von Zastrow M (2015). Effects of endocytosis on receptor-mediated signaling. Curr Opin Cell Biol 35, 137–143.
Kawabuchi M, Satomi Y, Takao T, Shimonishi Y, Nada S, Nagai K, Tarakhovsky A, Okada M (2000). Transmembrane phosphoprotein Cbp regulates the activities of Src-family tyrosine kinases. Nature 404, 999–1003.
Lemmon MA, Freed DM, Schlessinger J, Kiyatkin A (2016). The dark side of cell signaling: positive roles for negative regulators. Cell 164, 1172–1184.
Lemmon MA, Schlessinger J (2010). Cell signaling by receptor tyrosine kinases. Cell 141, 1117–1134.
Lindquist S, Karitkina D, Langnaese K, Posevitz-Fejfar A, Schraven B, Xavier R, Seed B, Lindquist JA (2011). Phosphoprotein associated with glycosphingolipid-enriched microdomains differentially modulates Src kinase activity in brain maturation. PLoS One 6, e23978.
Lindquist JA, Simeoni L, Schraven B (2003). Transmembrane adapters: attractants for cytoplasmic effectors. Immunol Rev 191, 165–182.
Liu P, Begley M, Michowski W, Inuzuka H, Ginzberg M, Gao D, Tsou P, Gan W, Papa A, Kim BM, *et al.* (2014). Cell-cycle-regulated activation of Akt kinase by phosphorylation at its carboxyl terminus. Nature 508, 541–545.
Manning BD, Toker A (2017). AKT/PKB signaling: navigating the network. Cell 169, 381–405.
Marlin MC, Li G (2015). Biogenesis and Function of the NGF/TrkA Signaling Endosome. Int Rev Cell Mol Biol 314, 239–257.
Marshall CJ (1995). Specificity of receptor tyrosine kinase signaling: Transient versus sustained extracellular signal-regulated kinase activation. Cell 80, 179–185.
Mayer BJ (2015). The discovery of modular binding domains: building blocks of cell signalling. Nat Rev Mol Cell Biol 16, 691–698.
McAlister GC, Huttlin EL, Haas W, Ting L, Jedrychowski MP, Rogers JC, Kuhn K, Pike I, Grothe RA, Blethrow JD, Gygi SP (2012). Increasing the multiplexing capacity of TMT using reporter ion isotopologues with isobaric masses. Anal Chem 84, 7469–7478.
McAlister GC, Nusinow DP, Jedrychowski MP, Wühr M, Huttlin EL, Erickson BK, Rad R, Haas W, Gygi SP (2014). MultiNotch MS3 enables accurate, sensitive, and multiplexed detection of differential expression across cancer cell line proteomes. Anal Chem 86, 7150–7158.
McCaffrey G, Welker J, Scott J, van Der Salm L, Grimes ML (2009). High-resolution fractionation of signaling endosomes containing different receptors. Traffic 10, 938–950.
Miller FD, Kaplan DR (2001). Neurotrophin signalling pathways regulating neuronal apoptosis. Cell Mol Life Sci 58, 1045–1053.
Mou H, Smith JL, Peng L, Yin H, Moore J, Zhang X, Song C, Sheel A, Wu Q, Ozata DM, *et al.* (2017). CRISPR / Cas9-mediated genome editing induces exon skipping by alternative splicing or exon deletion. Genome Biol 18, 1–8.
Oneyama C, Hikita T, Enya K, Dobenecker MW, Saito K, Nada S, Tarakhovsky A, Okada M (2008). The lipid raft-anchored adaptor protein Cbp controls the oncogenic potential of c-Src. Mol Cell 30, 426–436.
Palacios-Moreno J, Foltz L, Guo A, Stokes MP, Kuehn ED, George L, Comb M, Grimes ML (2015). Neuroblastoma tyrosine kinase signaling networks involve FYN and LYN in endosomes and lipid rafts. PLoS Comput Biol 11, e1004130.
Paulo JA, O'Connell JD, Gygi SP (2016). A Triple Knockout (TKO) Proteomics standard for diagnosing ion interference in isobaric labeling experiments. J Am Soc Mass Spectrom 27, 1620–1625.
Pawson T (2004). Specificity in signal transduction: from phosphotyrosine-sh2 domain interactions to complex cellular systems. Cell 116, 191–203.
Pryor S, McCaffrey G, Young LR, Grimes ML (2012). NGF causes TrKA to specifically attract microtubules to lipid rafts. PLoS One 7, e35163.
Reinecke J, Caplan S (2014). Endocytosis and the Src family of non-receptor tyrosine kinases. Biomol Concepts 5, 143–155.
Rueden CT, Schindelin J, Hiner MC, DeZonia BE, Walter AE, Arena ET, Eliceiri KW (2017). ImageJ2: ImageJ for the next generation of scientific image data. BMC Bioinformatics 18, 1–26.
Saitou T, Kajiwara K, Oneyama C, Suzuki T, Okada M (2014). Roles of raft-anchored adaptor Cbp/PAG1 in spatial regulation of c-Src kinase. PLoS One 9, 1–13.
Sandilands E, Frame MC (2008). Endosomal trafficking of Src tyrosine kinase. Trends Cell Biol 18, 322–329.
Schwarz TJ, Ebert B, Lie DC (2012). Stem cell maintenance in the adult mammalian hippocampus: A matter of signal integration? Dev Neurobiol 72, 1006–1015.
Scott-Solomon E, Kuruvilla R (2018). Mechanisms of neurotrophin trafficking via Trk receptors. Mol Cell Neurosci 91, 25–33.
Sharpe JJ, Cooper TA (2017). Unexpected consequences : exon skipping caused by CRISPR-generated mutations. Genome Biol 18, 1240–1243.
Shipley MM, Mangold CA, Szpara ML (2016). Differentiation of the SH-SY5Y human neuroblastoma cell line. J Vis Exp e53193.
Solheim SA, Petsalaki E, Stokka AJ, Russell RB, Tasken K, Berge T (2008a). Interactions between the Fyn SH3-domain and adaptor protein Cbp/PAG derived ligands, effects on kinase activity and affinity. FEBS J 275, 4863–4874.
Solheim SA, Torgersen KM, Tasken K, Berge T, Taskén K, Berge T (2008b). Regulation of FynT function by dual domain docking on PAG/Cbp. J Biol Chem 283, 2773–2783.
Taelman VF, Dobrowolski R, Plouhinec JL, Fuentealba LC, Vorwald PP, Gumper I, Sabatini DD, De Robertis EM (2010). Wnt signaling requires the sequetration of glucogen synthase kinase 3 inside multivesicular endosomes. Cell 143, 1136–1148.

Tassew NG, Charish J, Shabanzadeh AP, Luga V, Harada H, Farhani N, D'Onofrio P, Choi B, Ellabban A, Nickerson PEB, *et al.* (2017). Exosomes mediate mobilization of autocrine Wnt10b to promote axonal regeneration in the injured CNS. Cell Rep 20, 99–111.

Theveneau E, Mayor R (2012). Neural crest migration: interplay between chemorepellents, chemoattractants, contact inhibition, epithelial-mesenchymal transition, and collective cell migration. Wiley Interdiscip. Rev Dev Biol 1, 435–445.

Ting L, Rad R, Gygi SP, Haas W (2011). MS3 eliminates ratio distortion in isobaric labeling-based multiplexed quantitative proteomics. Nat Methods 8, 937–940.

Vinyoles M, DelValle-Pérez B, Curto J, Viñas-Castells R, Alba-Castellón L, García de Herreros A, Duñach M (2014). Multivesicular GSK3 sequestration upon Wnt signaling is controlled by p120-catenin/cadherin interaction with LRP5/6. Mol Cell 53, 444–457.

Von Bartheld CS, Altick AL (2011). Multivesicular bodies in neurons: Distribution, protein content, and trafficking functions. Prog Neurobiol 93, 313–340.

Wang J, Chang Y-F, Hamilton JI, Wilkinson MF (2002). Nonsense-associated altered splicing. Mol Cell 10, 951–957.

Ye M, Lehigh KM, Ginty DD (2018). Multivesicular bodies mediate long-range retrograde NGF-TrkA signaling. Elife 7, 1–29.

Zheng Y, Zhang C, Croucher DR, Soliman MA, St-Denis N, Pasculescu A, Taylor L, Tate SA, Hardy WR, Colwill K, *et al.* (2013). Temporal regulation of EGF signalling networks by the scaffold protein Shc1. Nature 499, 166–171.